



Microstructural evolution during creep of lamellar eutectoid and off-eutectoid FeAl/FeAl₂ alloys

A. Schmitt^a, K.S. Kumar^b, A. Kauffmann^a, M. Heilmaier^{a,*}

^a Institute for Applied Materials (IAM-WK), Karlsruhe Institute of Technology (KIT), Karlsruhe, Germany

^b School of Engineering, Brown University, Providence, RI, USA

ARTICLE INFO

Keywords:

Aluminides
Creep
Electron microscopy
Scanning/transmission
Electron backscatter diffraction
Automotive uses

ABSTRACT

The creep behavior of a fully lamellar FeAl/FeAl₂ eutectoid alloy was shown to exhibit a minimum creep rate and the absence of a pronounced steady state regime. To reveal the underlying mechanisms of creep leading to the macroscopic response described above, comprehensive TEM investigation of several crept specimens were performed. In the early stages of creep, the FeAl phase primarily carries creep deformation by dislocation motion, whereas FeAl₂ remains mostly plastically undeformed, except in certain locations near colony boundaries where the lamellar structure is disrupted/absent. Within the colonies, where the lamellae are intact, deformation is accommodated at the FeAl/FeAl₂ interface, resulting in an increase in interface dislocations. This continues to be the case at the minimum creep rate. With further progression in creep, FeAl₂ begins to participate in the process of plastic deformation in a more substantive manner through twinning and slip, while FeAl continues to plastically deform and dynamically recover. Further beyond the minimum, the lamellar structure adjacent to the colony boundaries breaks down, and these areas become the primary contributors to creep and results in a continuous loss in creep resistance. Based on these observations in the fully lamellar material, the creep response of off-eutectoid Fe-58Al and Fe-62Al as well as single-phase FeAl₂ are explained.

1. Introduction

A lamellar eutectoid morphology of cubic FeAl (B2) and triclinic FeAl₂ (space group P $\bar{1}$) occurs for a binary Fe-60.9 at.% Al alloy [1,2] (hereafter designated Fe-61Al) in the Fe-Al-system. In a previous paper [3], we reported on the creep behavior of this alloy. Specifically, we showed that the creep rate as a function of strain (or time) exhibits a pronounced minimum and a conspicuous absence of steady state creep (Fig. 1a and b). The increase in creep rate beyond the minimum was attributed to a deterioration of the lamellar structure in the vicinity of colony boundaries. The presence of the two phases combined with a high interfacial area due to the lamellar morphology, however, precluded detailed understanding of the individual contribution of these microstructural features to the observed creep response in the early stages as well as at and just beyond the minimum.

Other materials with lamellar (or fibrous) microstructure such as NiAl-Ta or -(Cr,Mo) [4–7] and TiAl [8,9] also exhibit a minimum in the creep rate as a function of time and strain. In fully lamellar TiAl, it has been demonstrated that the minimum creep rate decreases with decreasing lamellar spacing [10,11]. Electron microscopy studies have been performed on crept fully lamellar TiAl to characterize the

deformed microstructure [10,12] to elucidate the dominant mechanisms and to understand the role of interfaces in generating dislocations as well as impeding dislocation motion. In the case of a fully lamellar FeAl/FeAl₂, the dominant creep mechanisms were, however, not unambiguously identified although several hypotheses were discussed in Ref. [3]. These include:

- i) Both phases contribute to the creep deformation from the beginning and the increase in creep rate beyond the minimum is due to degradation of the lamellar morphology only.
- ii) Initially, one of the two phases plastically deforms and the second phase only contributes to creep beyond the minimum resulting in the increase in strain rate. Further out in the process, lamellar degradation occurs.
- iii) Creep deformation is accommodated by only one phase throughout the entire experiment, and the degradation of the lamellae result in the increase in strain rate beyond the minimum.

In this paper, we report the results of a comprehensive electron microscopy study of post-crept specimens to unequivocally determine the dominant creep mechanisms before, at and after the minimum of

* Corresponding author.

E-mail address: martin.heilmaier@kit.edu (M. Heilmaier).

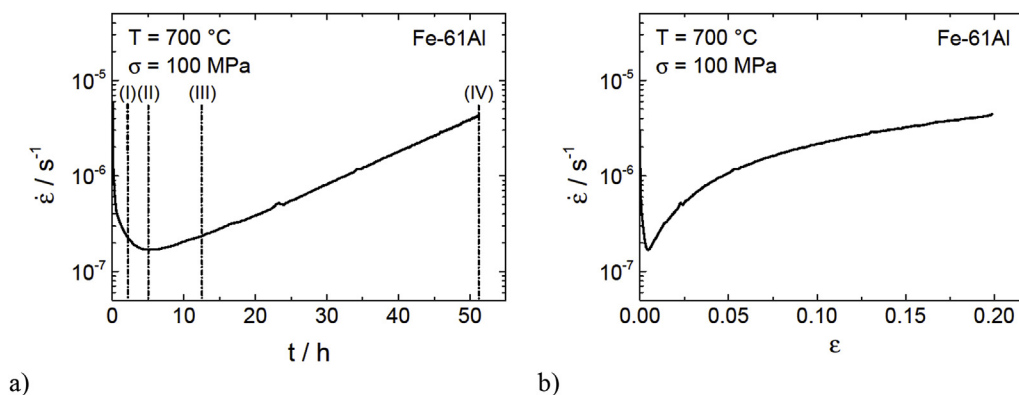


Fig. 1. (a) Creep rate versus time for a fully lamellar Fe-61Al and (b) creep rate versus strain. Dashed lines in (a) indicate times where additional tests were stopped for scanning electron microscopy (SEM) and transmission electron microscopy (TEM) investigations.

the strain rate as a function of time for the lamellar, eutectoid Fe-61Al alloy. The specific conditions examined are identified in Fig. 1a using dashed lines (I – IV). Observations are then used to interpret the creep response of the off-eutectoid alloys.

2. Experimental procedure

The Fe-61Al eutectoid alloy used in this study was produced by arc melting Al (99.99%) and Fe (99.99%) bulk elements. Single-phase FeAl₂ as well as off-eutectoid Fe-58Al and Fe-62Al (including pro-eutectoid FeAl and FeAl₂, respectively) were also similarly synthesized. Processing details for all of these alloys are provided in Ref. [3]. Cylindrical samples, 5 mm in diameter and 8 mm in height, were electrical discharge machined from the as-cast rod for creep experiments.

All samples were isothermally crept in compression at a constant true stress of 100 MPa at 700 °C in vacuum (pressure of about 10⁻³ Pa). Based on the observed minimum in the creep curve (Fig. 1a and b) for the eutectoid alloy, additional tests were performed on this alloy and interrupted after: (I) 2 h (early state of creep; prior to the minimum), (II) 5 h (minimum), (III) 12.5 h (beyond the minimum) and (IV) about 50 h to assess the microstructural evolution with creep strain.

Scanning electron microscopy (SEM) coupled with electron backscatter diffraction (EBSD) (Auriga 60, Zeiss) and electron channeling contrast was used to investigate the microstructure evolution in the deformed specimens. Specimens were embedded in a polymer matrix and prepared for observation using mechanical grinding followed by polishing with 1 μm diamond suspension. Final polishing was performed using a non-crystallizing oxide polishing suspension OP-S provided by Struers, Denmark.

Multiple disks, 3 mm in diameter and 1 mm in thickness, were sliced from the as-cast and the crept specimens by electrical discharge machining and mechanically ground to a final thickness of 150–180 μm. These discs were jet polished to perforation in a Tenupol-5 (Struers, Denmark) using 80 vol.% sulfuric acid and 20 vol.% methanol as electrolyte at 20 °C and at 17 V. A CM20 transmission electron microscopy (TEM) operating at 200 kV was used in the bright field mode to characterize the microstructure.

3. Results

An SEM image of the as-cast microstructure is shown in Fig. 2. This microstructure is described in detail elsewhere [3]. Briefly, the lamellar microstructure is fairly regular, and includes branching and termination of lamellae within the colonies. In the vicinity of colony boundaries however, irregularities were observed including the presence of 1–5 μm single-phase regions resulting from the lamellae not quite reaching the boundary. At the eutectoid temperature of 1095 °C, the Fe-61Al alloy contains 30.0 vol.% of FeAl as determined from the phase diagram

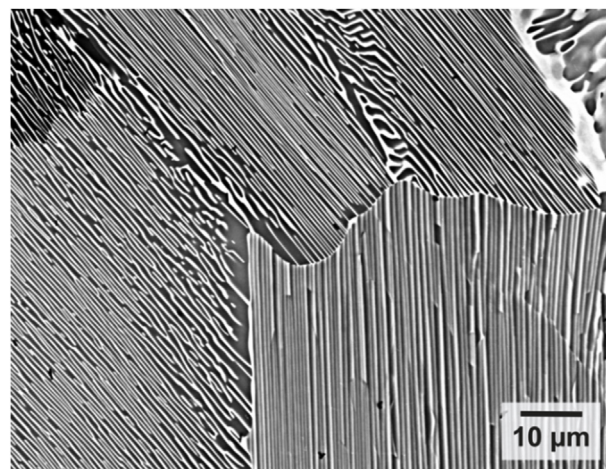


Fig. 2. SEM micrograph of the as-cast microstructure. Bright phase is FeAl; dark phase is FeAl₂ while grey scale differences within FeAl₂ indicate orientation change between the colonies due to channeling contrast.

provided in Ref. [1] and using crystallographic data from Ref. [13]. The calculated volume fraction only changes marginally to 29.9 vol.% FeAl in the proximity of the creep test temperature of 700 °C. Even cooling down to room temperature only results in a small shift in the relative amounts of the co-existing phases (27.6 vol.% FeAl). Hence, even though the alloys were creep tested at 700 °C in the as-cast condition, changes in volume fraction of the co-existing phases are not anticipated during the isothermal creep test.

A set of bright-field TEM images describing the as-cast lamellar microstructure is presented in Fig. 3. In Fig. 3a, a representative region from the interior of a colony is shown. The phase in dark contrast is FeAl while the lighter contrast lamellae flanking it on either side are FeAl₂. Multiple FeAl lamellae terminations are evident and antiphase boundaries (APB) are seen emanating frequently from these terminations (highlighted by white arrows in Fig. 3a) and traversing the FeAl₂ lamellae. A higher magnification image of these APBs is shown in Fig. 3b. During the eutectoid decomposition of Fe₅Al₈ on cooling, cooperative growth of lamellar FeAl and FeAl₂ occurs, typically commencing from a grain boundary. When an FeAl lamella terminates, it will result in the impingement of the two adjacent FeAl₂ lamellae (due to distinct orientation relation with similar crystallographic disposition [14]) within the single colony. This impingement can produce one or more APBs in the triclinic structure as a way to accommodate orientation and/or translation discrepancy.

Tilting experiments confirmed a low dislocation density in both phases (few can be seen in FeAl₂ in Fig. 3a). The observed dislocation

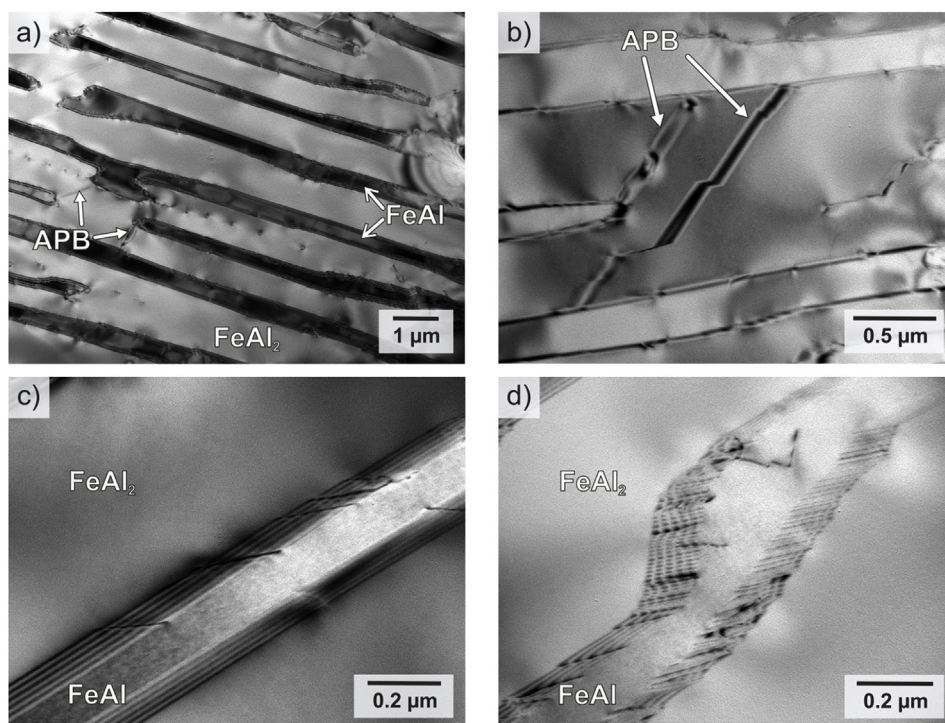


Fig. 3. TEM micrographs of as-cast Fe-61Al. FeAl and FeAl₂ are almost free of dislocations. A few APBs (highlighted by white arrows) are noted at terminations and branches in (a). The characteristic fringe contrast observed supports the presumption of APB formation (b). Dislocations are present at the FeAl/FeAl₂ interfaces in (c) and (d), the average spacing being larger in the straight sections (c) as compared to the curved locations (d).

density at the FeAl/FeAl₂ lamellar interface depends on whether the interface is straight or curved (see Fig. 3c and d). Given the orientation relationship, the habit plane and the low misfit (0.14% maximum) [14], it is reasonable to expect a large average spacing between misfit dislocations at the interface; interface curvature (at terminations and junctions and/or when the lamellae are bent) appears to be accommodated with additional dislocations resulting in a reduced average dislocation spacing. The average distance of interface dislocations in locations is about $(0.9 \pm 0.3) \mu\text{m}$, where the interface is straight. SEM examination confirmed the absence of other microstructural features like subgrains or twins in the initial state.

An SEM micrograph obtained using electron channeling contrast of the lamellar alloy that had been crept for 2 h to a true plastic strain of 0.2% at 700 °C at 100 MPa (vertical line I in Fig. 1a) is shown in Fig. 4a. No changes are observed relative to the initial microstructure. Electron channeling contrast imaging enables identification of subgrains and/or twins that might have developed during deformation but neither of those are present.

The microstructure in this condition was examined by TEM and representative images are shown in Fig. 4b–e. Fig. 4b and c are from locations within the colony where well-aligned lamellae are present and exhibit spacing is close to the average spacing of $(380 \pm 40) \text{nm}$ [15]. Fig. 4d represents a location in the vicinity of a colony boundary where a FeAl lamella has terminated, leaving behind a fairly large single-phase FeAl₂ region. Fig. 4e is a higher magnification image of the location identified in Fig. 4d by the dashed white rectangle.

The bright field image in Fig. 4b confirms that FeAl has experienced local plastic deformation evidenced by the dislocations within these lamellae. Furthermore, subgrains indicative of dynamic recovery are observed in FeAl as well (Fig. 4d and e). In contrast, the FeAl₂ phase seems to be mostly free of dislocations (Fig. 4b and c). The dislocation density at the FeAl/FeAl₂ interfaces appears to have increased and measurements confirm that their average spacing is $(0.5 \pm 0.3) \mu\text{m}$ (Fig. 4f). In other locations where the lamellar microstructure is disrupted, some dislocations are observed in FeAl₂ (marked by white dashed circles in Fig. 4d). Also prominent is the presence of well-defined subgrains, some of which are numbered from 1 to 4 in Fig. 4d.

These microstructural features indicate that in this early stage, FeAl

plastically deforms and carries the creep strain. Within the colonies where the lamellar structure is preserved, the resulting shape change is accommodated through an increase in the interface dislocation content and the elastic deformation of FeAl₂. In the vicinity of colony boundaries, where the lamellar structure is disrupted due to termination of the FeAl lamellae, FeAl₂ has dynamically recovered which is indicative of local plastic deformation. These microstructural footprints imply significant inhomogeneous strain distribution during high-temperature deformation. Such inhomogeneity can be attributed to the spatially changing microstructural constraints within a colony as well as to the variation in lamellar orientation with respect to the loading axis from colony to colony.

After 5 h at 700 °C (at 100 MPa), the specimen exhibits a true plastic strain of ~0.5% and minimum creep rate is achieved (vertical line II in Fig. 1a). The corresponding microstructure does not exhibit significant differences compared to the microstructure of the specimen crept for 2 h which was discussed above (see Figs. 4a and 5a). Dislocations are readily seen in the FeAl lamellae whereas this is not evident in FeAl₂ (Fig. 5b and c). Also, the FeAl/FeAl₂ interface dislocation spacing changes only marginally compared to that stated for the 2 h specimen.

Thus, for creep times/strains prior to and at the minimum, within the colonies where the lamellar structure is regular, FeAl is the predominant plastically deforming phase while FeAl₂ deforms elastically. Interface compatibility is accommodated through an increase in interface dislocations. However, an increased dislocation density in FeAl and at the interphase interfaces can result in increased internal stress and strain that together with the externally applied stress, has the potential to trigger plastic deformation in the FeAl₂ lamellae as well. In the vicinity of colony boundaries where the lamellar structure is disrupted, dynamic recovery of FeAl₂ was noted, suggesting local plastic deformation.

The sample crept for 12.5 h corresponds to the vertical line III marked in Fig. 1a. This condition is therefore beyond the minimum in the creep curve. A SEM image obtained using electron channeling contrast (Fig. 6a) confirms the presence of planar interfaces within the FeAl₂ phase that are twins (see EBSD analysis in Fig. 7). Representative TEM bright field images provided in Fig. 6b–d illustrate twin contrast in several of the FeAl₂ lamellae and these twins seem to terminate on

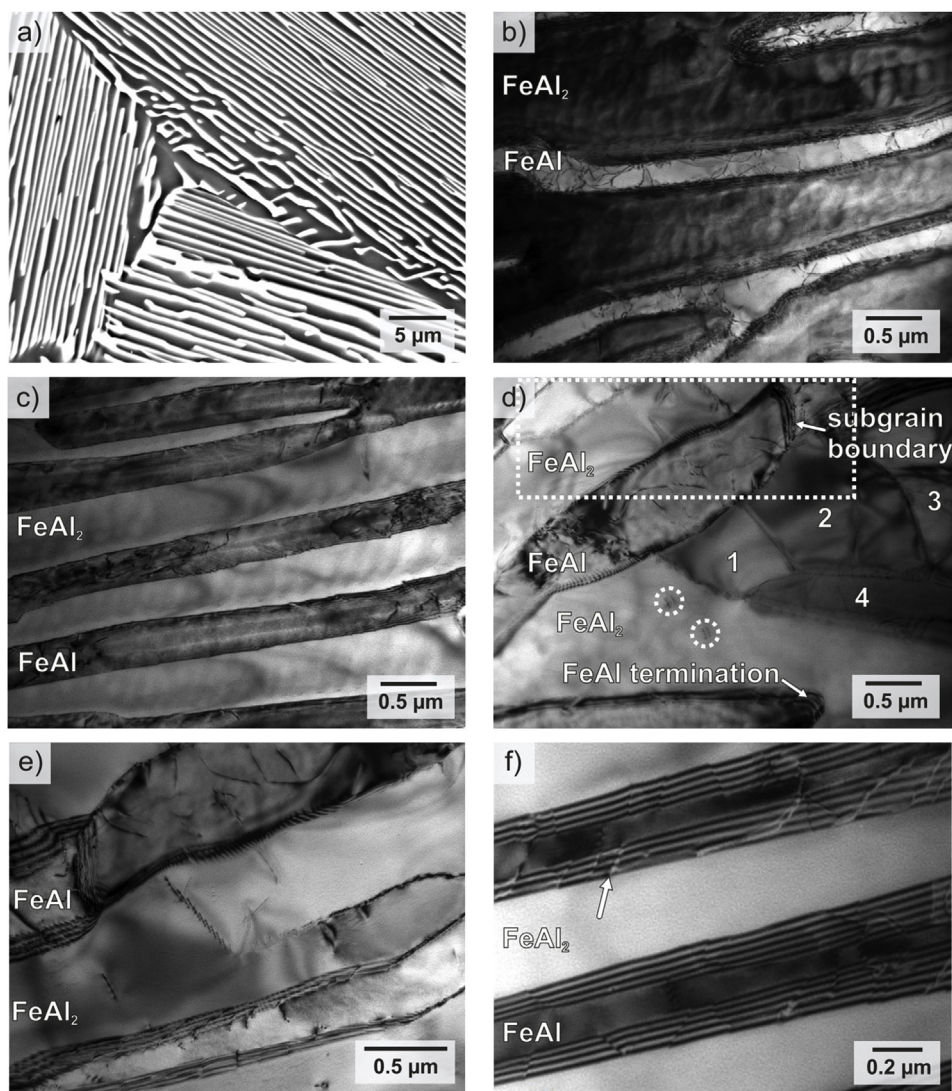


Fig. 4. (a) SEM micrograph of a crept sample at 700 °C and 100 MPa for 2 h (~0.2% true plastic strain) showing the lamellar structure as well as colony boundaries and obtained using electron channeling contrast. The bright phase is FeAl and the dark phase is FeAl₂. The periodicity of the lamellar structure is disrupted in the vicinity of the colony boundaries. (b–e) are TEM micrographs of the same deformed specimen. In (b), dislocations are seen in FeAl but not in FeAl₂ providing evidence for the sole plastic deformation of FeAl. Reversing the phase contrast in (c) by tilting confirms that dislocations are still not visible in FeAl₂. (d,e) show the presence of subgrain boundaries in FeAl as well as dislocations and subgrains in FeAl₂ (marked 1–4 in (d)) where the lamellar structure is disrupted. In (f), a high magnification image shows interface dislocations (for example highlighted by an arrow).

adjacent FeAl/FeAl₂ interfaces. To the best of our knowledge, this is the first report of deformation twinning in the triclinic FeAl₂ phase. In other locations, twins originate from the interface but do not completely traverse the FeAl₂ lamella, confirming that the interface is likely a nucleation site for these twins (Fig. 6c and d).

The specimen crept for 12.5 h exhibits a true strain of ~2% and a large part of this strain is accommodated by plastic deformation of FeAl accompanied by significant increase in interface dislocation content. The average dislocation spacing is $(0.08 \pm 0.03) \mu\text{m}$ as compared to $(0.3 \pm 0.1) \mu\text{m}$ at the minimum creep rate (Fig. 6f). It is conceivable that the internal stress arising from these interface dislocations in conjunction with the externally applied 100 MPa stress provides the driving force for generating twins in FeAl₂ from FeAl/FeAl₂ interfaces. Previously, it has been shown that interfaces in lamellar structures can indeed be twin nucleation sites in the TiAl/Ti₃Al system [16].

In other locations in the 12.5 h specimen, individual dislocations are observed in both, FeAl₂ and FeAl lamellae, implying slip plays a role as well in the plastic deformation of both phases (Fig. 6c–e). In a previous study [14], it was shown that the (114)[1 $\bar{1}$ 0], ($\bar{1}\bar{1}$ 3)[1 $\bar{1}$ 0] and (221)[1 $\bar{1}$ 0] of FeAl₂ exhibit similar atomic arrangement as the {1 $\bar{1}$ 0} <111> in the B2 FeAl representing the potential slip system family in the latter [17–19]. Therefore, it is possible that the observed dislocations in FeAl₂ in Fig. 6c–e could be related to one or more of these slip systems.

In order to confirm the presence of deformation twins in FeAl₂ as described above, orientation imaging microscopy by EBSD was

performed. An orientation map obtained from a cross section of the 12.5 h crept material is shown along with an image quality map in Fig. 7a and b. There are frequent orientation changes observed within the FeAl₂ phase which are separated by planar interfaces (examples of which are highlighted by green arrows in Fig. 7a). According to EBSD, the orientation change corresponds to a 180° rotation about a [$\bar{1}\bar{3}$ 0 27] crystallographic direction, confirming the twin characteristic of the interface. A stereographic projection illustrating the matrix/twin orientation relationship in the FeAl₂ phase is provided in Fig. 8. Note that the [$\bar{1}\bar{3}$ 0 27] crystallographic direction is the plane normal of the (001) plane in this triclinic unit cell. It is highlighted by bold font as the rotation axis of the twins. According to the stereographic projection of the matrix and twin, the crystallographic directions [100], [010] as well as the special direction [1 $\bar{1}$ 0] (see Ref. [14]) are reversed since these crystallographic directions are within the (001) plane. Furthermore, the relatively close packed (see Ref. [14]) planes (114) and ($\bar{1}\bar{1}$ 3) are added. These planes are inverted by the twin transformation in the sense that a (114) plane in the matrix is parallel to a ($\bar{1}\bar{1}$ 3) in the twin and vice versa. The plane normal of the third rather close packed plane (221) of the FeAl₂ structure lies within the (001) plane and is accordingly just reverted to ($\bar{2}\bar{2}\bar{1}$).

In order to identify the most probable twinning plane, the primary twins were analyzed (see Fig. 7a green arrows). The intersections of the twin boundaries with the surface are highlighted by a green dotted line in Fig. 7a which is rotated about $(51 \pm 2)^\circ$ with respect to the

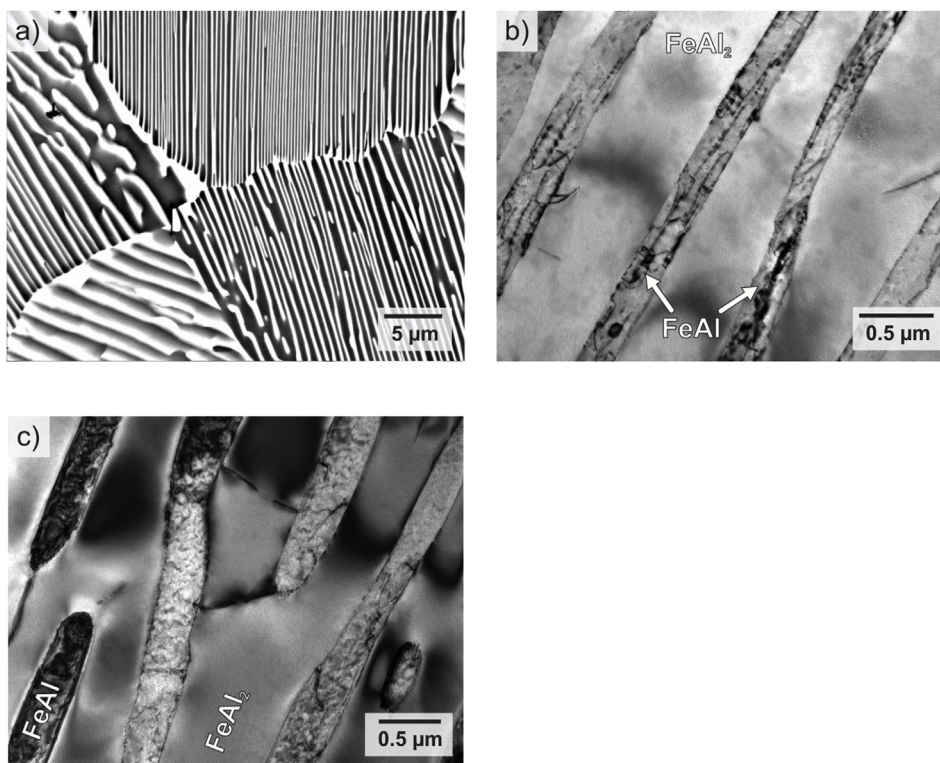


Fig. 5. At the minimum creep rate (5 h of deformation at 700 °C, 100 MPa, true plastic strain of $\sim 0.5\%$): (a) SEM as well as (b,c) TEM micrographs show plastic deformation of FeAl lamellae but not of FeAl₂. This is similar to the observations made for the 2 h exposure specimen.

horizontal image axis. Since depth information is missing, a line crossing the center has to be included in the stereographic projection in Fig. 8. The corresponding green dotted line intersects the plane normal of (001). Thus, (001) is the most probable twin plane of the primary twin system in the present case.

The last specimen examined in this study was crept for ~ 50 h at 700 °C at a constant true stress of 100 MPa (vertical line IV in Fig. 1a). This long term exposure results in $\sim 20\%$ plastic strain and representative SEM micrographs of this microstructure are presented in Fig. 9a and b that correspond to the colony interior (a) where the lamellar structure is fairly well preserved and in the vicinity of the colony boundary (Fig. 9a) (b) where the initial microstructure visibly breaks down (Fig. 9b). In Fig. 9b, contrast arising from crystallographic orientation enables identification of subgrains in both constituent phases. TEM examination of regions in the vicinity of colony boundaries (Fig. 9c) confirms the SEM observations. There is a substantial breakdown of the lamellar morphology and subgrain formation. The large creep strain experienced by this specimen is accommodated by plastic deformation in both phases (slip in FeAl, slip and twinning in FeAl₂) and quite likely some interface sliding. Within the individual FeAl₂ lamellae, deformation twins are present (Fig. 9d). The relatively large offsets of roughly 300 nm (highlighted in Fig. 9d) are indicative of sliding along these twin boundaries. The possibility for twin boundary sliding was recently revealed for pure Cu [20]. In this case, the twin boundary does not migrate as it is expected for the motion of twinning dislocations within the twinning plane. Instead, a dislocation source (with a Burgers vector different to the one of twinning dislocations) is active within the boundary and provides displacement of twin and matrix with respect to each other [20]. The development of subgrain boundaries in both phases as well as twin boundaries in FeAl₂ all of which intersect the FeAl/FeAl₂ interfaces contribute to cusping of otherwise straight lamellar interfaces (due to the need to maintain interfacial energy balance) that can set the stage for subsequent breakdown of the lamellae. The average dislocation spacing is (0.08 ± 0.03) μm and comparable to the one crept for 12.5 h (Fig. 9e).

In order to demonstrate that the degradation of the lamellae after 50 h reported above is not solely due to thermal exposure (i.e. it is due to creep), an unloaded sample heat-treated for 50 h at 700 °C was examined as well. The resulting microstructure is shown in Fig. 10. It is evident that the initial, lamellar microstructure is still intact (Fig. 10a) although there is some increase in the average lamellar spacing [3]. No subgrains are found in FeAl or FeAl₂ and the microstructure in the vicinity of the colony boundaries does not appear to be visibly degraded (Fig. 10b). Hence, we conclude that degradation of the lamellar structure is primarily caused by the combined effect of stress, temperature and time and is not just related to isothermal coarsening.

4. Microstructural-based interpretation of isothermal creep response of the eutectoid FeAl-FeAl₂ alloy

The intent of this experimental effort was to provide a microstructure-based understanding for the observed creep response of the lamellar FeAl/FeAl₂ eutectoid alloy at 700 °C and a constant stress of 100 MPa. The study has shown that during deformation under the prescribed conditions, the FeAl phase begins to plastically deform first by dislocation motion. The process is constrained by FeAl₂ and the discrepancy in deformation is accommodated by an increase in interface dislocations. As the process evolves, FeAl₂ commences plastic deformation by twinning and slip. Although the lamellar microstructure within the individual colonies in the as-cast condition is regular, the structure periodicity is frequently disrupted in the vicinity of colony boundaries. In such locations, subgrains within the constituent phases developed during creep, suggesting locally larger plastic strain and dynamic recovery. At later stages, breakdown of the lamellar structure occurs, particularly in regions close to colony boundaries.

Larger strains (for example $> 15\%$) will require colony shape change to account for the axial strain and this should be accompanied by lamellae stretching and rotation (Fig. 11a). Plastic deformation of FeAl lamellae primarily proceeds by dislocation activity while in FeAl₂ both slip and twinning continue (see Fig. 6b–d). The localization of

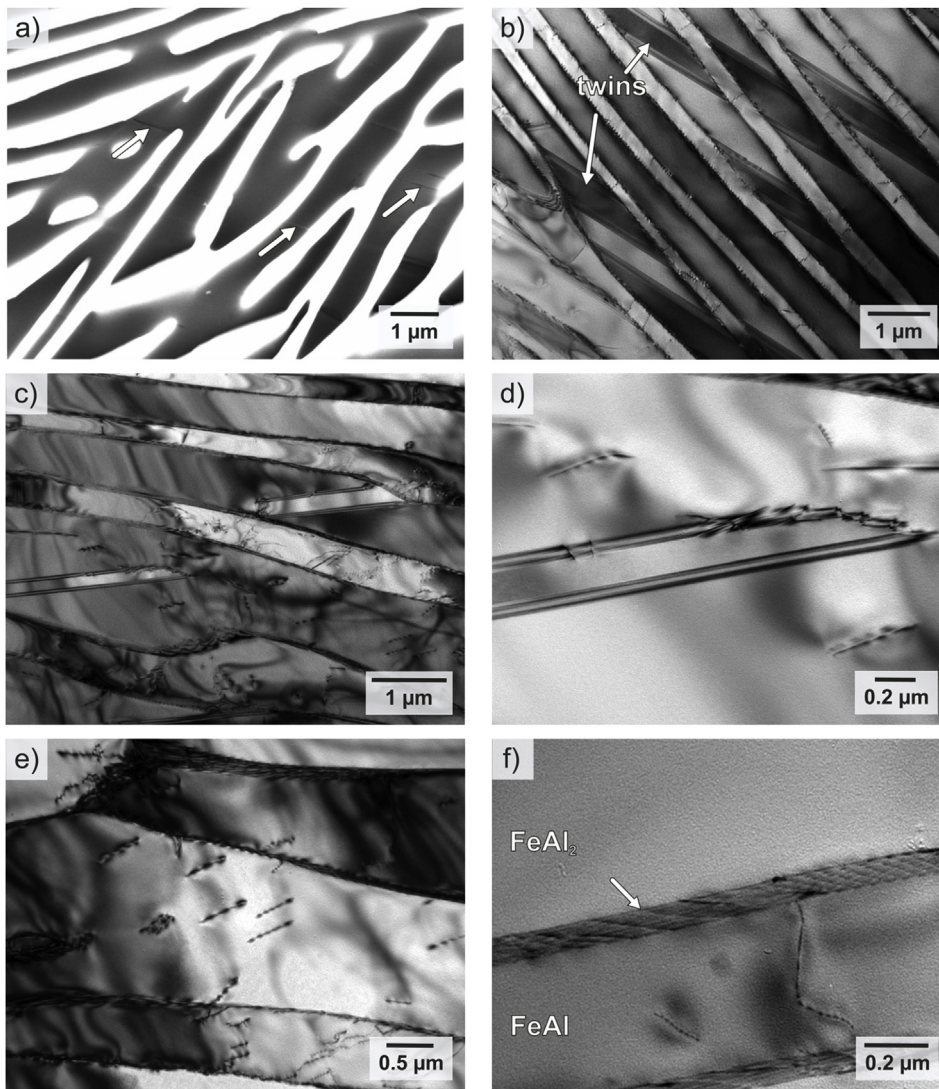


Fig. 6. Microstructure after 12.5 h exposure to 700 °C at 100 MPa and a true plastic strain of ~2%. (a) SEM and (b–d) TEM micrographs showing twins in the FeAl₂ phase in lamellar regions. In (b) the twins completely traverse the FeAl₂ lamellae whereas in (c) the twins start from the FeAl/FeAl₂ interface but terminate within the FeAl₂ lamellae; in (d), a high magnification image of the twin termination is shown for one such instance. Dislocation activity in the FeAl₂ phase is illustrated in (e). A high magnification image of the interface is shown in (f) and represents one of several from which the average dislocation spacing of (0.08 ± 0.03) μm was measured. An interface dislocation is highlighted by an arrow.

these deformation modes can destabilize the lamellar morphology.

The lamellar orientation incompatibility at colony boundaries will also result in considerable localization of stress developing at the colony boundaries in the vicinity of such boundaries leading to lamellae bending and polygonization (Fig. 11b). This will lead to destabilization of the lamellae and the formation of rather equiaxed grains of FeAl and

FeAl₂ adjacent to the colony boundaries as was observed in the 50 h specimen in Fig. 9b and c. These microstructural instabilities account for the loss in creep resistance (i.e. increased creep rate with strain and/or time) of the composite.

Previously, stress exponents in the range of 3–4 were reported for isothermal creep (700 °C) of polycolony, lamellar FeAl/FeAl₂ alloys [3].

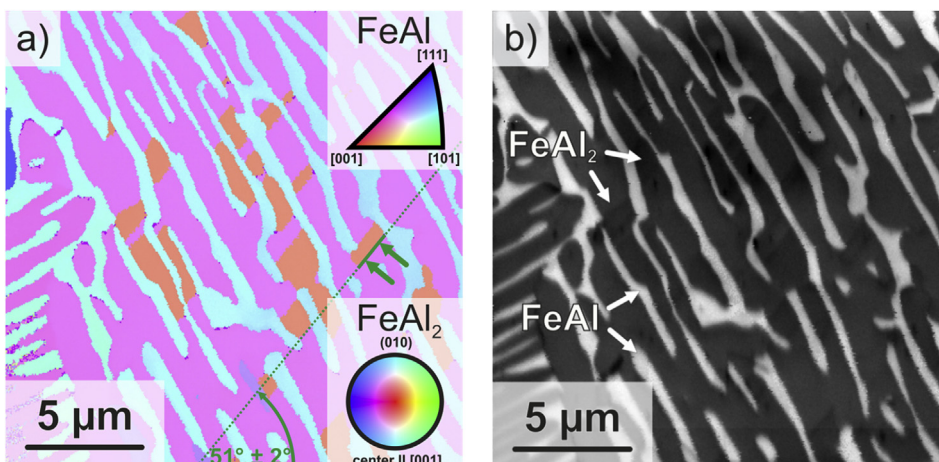


Fig. 7. Orientation imaging microscopy by EBSD on a cross section of material crept for 12.5 h at 100 MPa: (a) orientation map (color-coding according to the inverse pole figures of the compression direction in the insets) showing a pink colored FeAl₂ matrix including orange colored twins. Green arrows highlight a straight twin boundary (in-plane orientation of the primary twin system is denoted by a dotted line), (b) image quality map. (For interpretation of the references to color in this figure legend, the reader is referred to the web version of this article.)

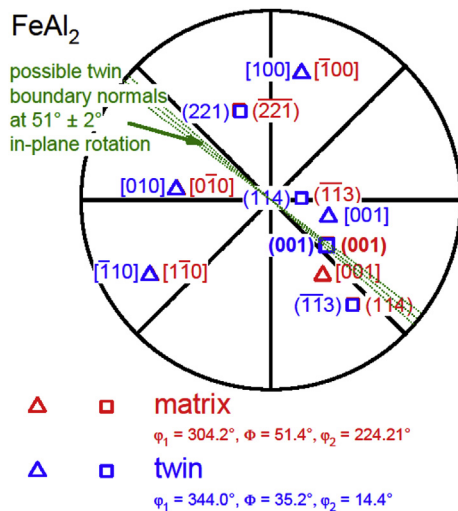


Fig. 8. Stereographic projection of the orientations obtained in Fig. 7a (Eulerian angles in Bunge notation) including the possible twin plane normals from the cross section highlighted by dotted lines. Triangles denote crystallographic directions and squares denote plane normals. The identified twin rotation axis (001) is highlighted in bold and intersects with the possible twin plane normal.

These values usually imply dislocation glide and climb controlled creep which electron microscopy now substantiates. Measured and reported activation energies for creep at the minimum creep rate ($Q = 321 \pm 26$ kJ/mol [3]) and at 4% creep strain which is beyond the minimum ($Q = 338 \pm 21$ kJ/mol [3]) are however more difficult to associate with deformation microstructure. This is due to multiple microstructural features such as co-existing phases and their lamellar morphology, interfaces and colony boundaries participating collectively in creep. Such a hierarchical microstructure leads to inhomogeneous strain distribution and plastic flow in one or more phases within the colonies, possible lamellar interface sliding, and dynamic recovery of the constituent phases in the vicinity of colony boundaries exacerbating the situation, thereby precluding a meaningful mechanistic description of the apparent activation energy.

We further examine the observed creep response in Fig. 1a and b in the context of the creep behavior of single-phase FeAl and FeAl₂ under similar conditions (Fig. 12). The single-phase FeAl is significantly weaker in creep relative to single-phase FeAl₂ while the minimum creep rate for the lamellar eutectoid alloy is similar to that for single-phase FeAl₂. The stress exponent of slightly above 3 for FeAl₂ in Ref. [3] as well as for FeAl in Ref. [21] indicates dislocation-based creep in both cases. Even though dislocation creep dominates in both single phase material, the associated creep transient is rather small (within one order of creep rate in both cases) suggesting low work-hardening capacity in either of these phases. In contrast, the eutectoid alloy possesses a pronounced creep transient (two orders of magnitude in creep rate). This significant initial decrease in creep rate in the lamellar alloy is thought to result from the fact that until the minimum creep rate is reached, FeAl is the primary carrier of plastic deformation by dislocation motion within the lamellar regions. The constraints imposed by the elastic response of FeAl₂ in a lamellar morphology discourage the evolution of plastic strain in FeAl and consequently enhances the work-hardening rate of the composite. Thus, the reacceleration of creep (and hence the presence of a minimum in creep rate) is thought to be determined by the onset of plastic deformation of FeAl₂ as confirmed experimentally by the appearance of dislocation motion and twinning in that phase beyond the creep rate minimum. The observed increase in interfacial dislocation content in the early stages of deformation also reflects the mechanical incompatibility between these two phases. Close to colony boundaries where the lamellar structure is absent, FeAl₂ subgrains reveal dynamic recovery suggesting previously locally high

plastic strain gradients (that drives the recovery process locally) possibly arising from adjacent, differently oriented colonies (Fig. 11b).

With further deformation (beyond the minimum in Fig. 1a and b), the critical stress for twinning in FeAl₂ is reached and plastic deformation of this phase commences by slip and twinning, reducing the previous elastic constraint and resulting in an acceleration of creep rate of the composite. The twins appear to emanate from the FeAl/FeAl₂ interfaces, likely encouraged by the local stresses arising from the increased dislocation content at these interfaces. The twin plane in triclinic FeAl₂ was shown to be of (001) type. EBSD analyses of the deformed single-phase FeAl₂ also confirmed twinning to be an important deformation mode at 700 °C. An example for a bundle of deformation twins (note the lenticular shape) is shown in Fig. 13. Several deformation twins in various grains were analyzed with respect to their orientation relation and possible twin plane in a similar manner to the analysis in Figs. 7 and 8. In all cases, rotations of 179.9–180° about $[\bar{1}02]$, $[5011]$ as well as $[\bar{6}013]$ crystallographic directions were identified. All detected directions are close to each other (maximum deviation of 1.5°) and similar to the $[\bar{1}\bar{3}027]$ (maximum deviation of 0.9°) as found for the twins in the crept lamellar material (Figs. 7 and 8). Furthermore, the observed traces of the twin boundaries on the cross sections coincide with the potential (001) twinning plane. Therefore, we conclude that the observed deformation twin systems in the single-phase material and the lamellar, multi-phase alloy are the same. Discontinuities such as the phase boundaries in the lamellar, eutectoid alloy as well as grain boundaries and cracks in single-phase FeAl₂ were found to be favorable twin initiation sites. Thus, the observed enhancement in creep rate at the macroscopic level is attributed to the beginning of significant plastic deformation of FeAl₂.

5. Interpretation of the creep response of off-eutectoid Fe-58Al and Fe-62Al

The microstructural explanation for the creep response of the eutectoid alloy Fe-61Al which has been the focus of this work can also be extended to off-eutectoid alloys. Thus, the creep response at 700 °C and a constant stress of 100 MPa for Fe-58Al and Fe-62Al as previously reported in Ref. [3] are compared to that for the eutectoid alloy Fe-61Al in Fig. 14. The higher minimum creep rates observed in both Fe-58Al (FeAl pro-eutectoid phase) and Fe-62Al (FeAl₂ pro-eutectoid phase) relative to the eutectoid alloy are of relevance here.

The higher minimum creep rate observed for the Fe-58Al alloy relative to the fully lamellar Fe-61Al alloy is not altogether surprising, considering there is a substantial amount of the less creep-resistant FeAl phase present, both, as globular pro-eutectoid FeAl and as constituent of the eutectoid microstructure within the lamellar morphology [3]. The observation of deformation twins in the FeAl₂ phase in the Fe-58Al alloy crept beyond the minimum (Fig. 15a and b) suggests once again that the minimum can be correlated to the onset of plastic deformation of FeAl₂.

It is, however, rather surprising that the minimum creep rate recorded for the Fe-62Al is higher than that of the eutectoid alloy (Fig. 14) since the pro-eutectoid phase is FeAl₂ which is more creep resistant than FeAl (Fig. 12). A careful examination of the microstructure of a Fe-62Al specimen crept beyond the minimum (Fig. 15c and d) confirms: (i) the presence of a continuous network of FeAl around individual blocks of FeAl₂ and (ii) the presence of twins within these FeAl₂ blocks. Such a continuous network of the weaker FeAl phase can explain the loss in creep resistance while the presence of twins in FeAl₂ is consistent with the assumption that the minimum is associated with onset of plastic deformation in the FeAl₂ phase. At larger strain, Fe-62Al exhibits a lower creep rate relative to Fe-61Al, suggestive of less microstructure destabilization in the former. This is likely due to the reduced fraction of lamellar regions (by volume) and possible rupturing of the continuous network of FeAl due to localized plastic deformation of the blocky FeAl₂ by twinning. The twins typically

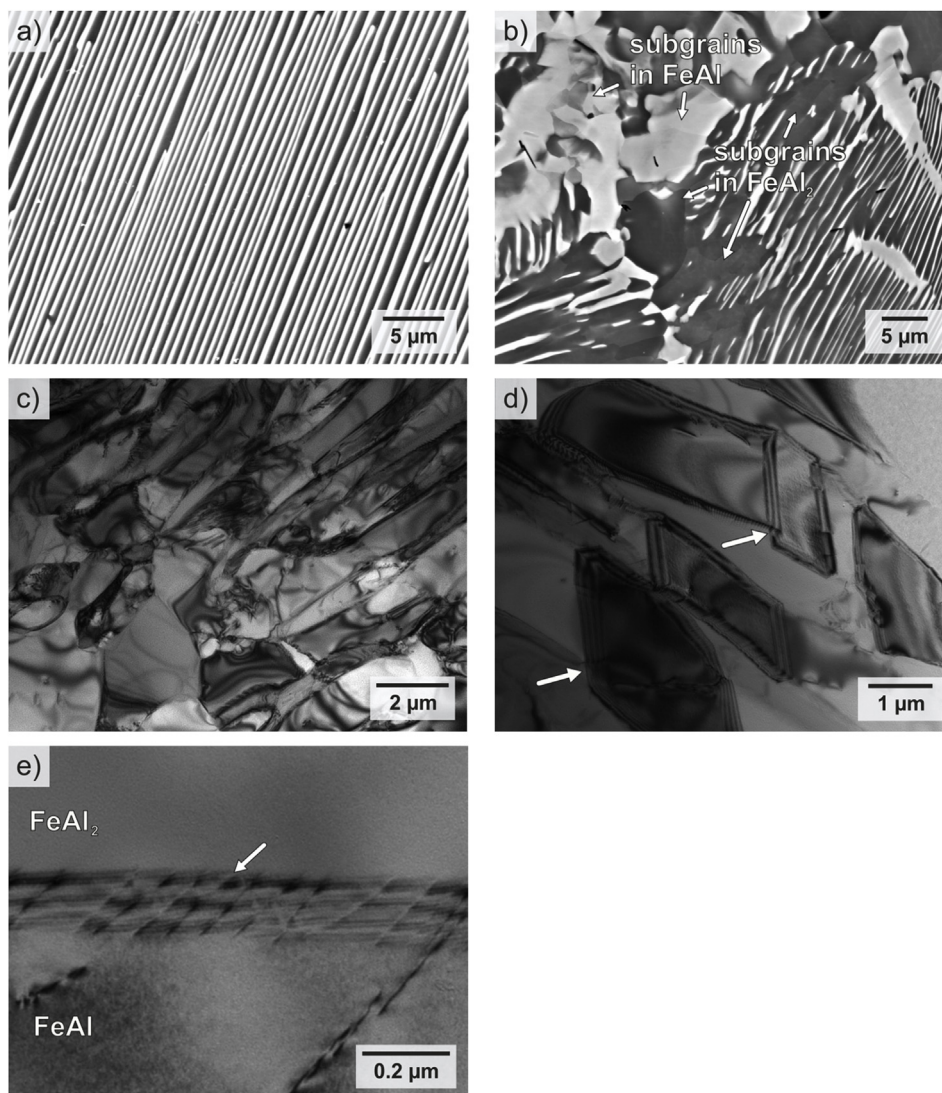


Fig. 9. SEM micrographs of the 50 h crept sample: (a) the lamellae in the colony are still straight and fine whereas, and (b) substantial degradation of the lamellar structure is evident in the vicinity of colony boundaries. TEM bright field images of the same sample: (c) in the vicinity of a colony boundary showing subgrains in both phases and lamellar morphology breakdown, and (d) twins in FeAl₂ and sliding along the twin boundary indicated by steps (highlighted by arrows). The measured average dislocation spacing is comparable to the specimen crept for 12.5 h; an example shown in (e) (an interface dislocation is highlighted by an arrow).

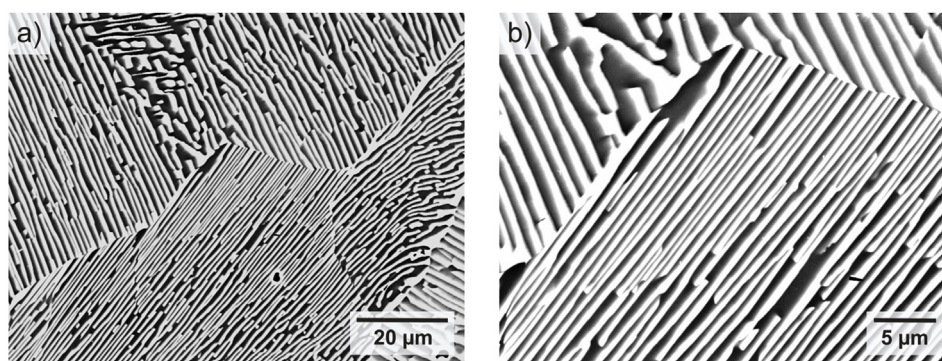


Fig. 10. (a) SEM micrograph of a 50 h at 700 °C heat-treated material and (b) a higher magnification of a colony boundary from (a).

terminate at the FeAl/FeAl₂ interface which results in localized deformation of FeAl (highlighted with white arrows in Fig. 15c). Hence, the surrounding continuous FeAl phase will break off and consequently more continuous regions of pro-eutectoid FeAl₂ prevail.

6. Conclusion

The underlying mechanism(s) governing the isothermal creep response at 700 °C and 100 MPa of eutectoid FeAl/FeAl₂ with a lamellar microstructure has/have been revealed by using electron microscopy to

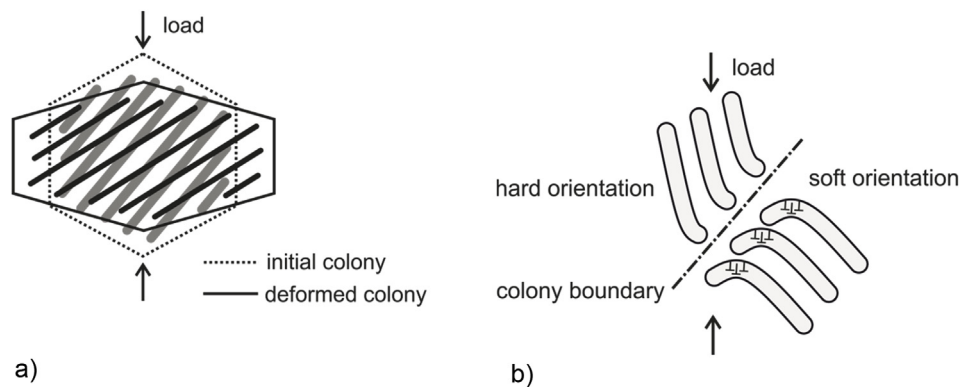


Fig. 11. Schematic illustration of (a) the colony shape change associated with creep deformation and the associated elongation and rotation of the lamellae and (b) two adjacent colonies exhibiting a “soft” and “hard” orientation relative to the loading axis, resulting in a locally high, plastic strain gradient.

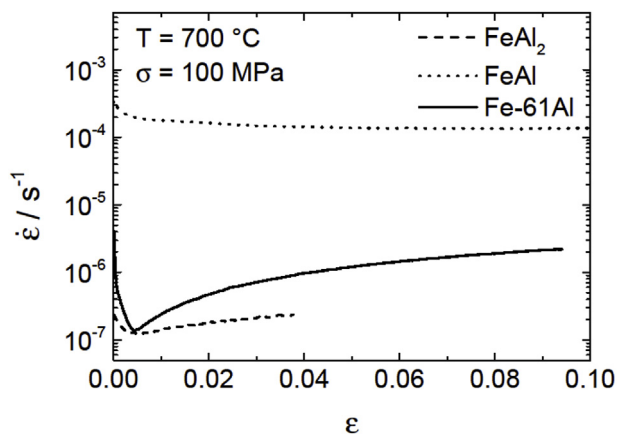


Fig. 12. Creep curves of single-phase FeAl and FeAl₂ as well as fully lamellar Fe-61Al at 700 °C and an applied true stress of 100 MPa [3].

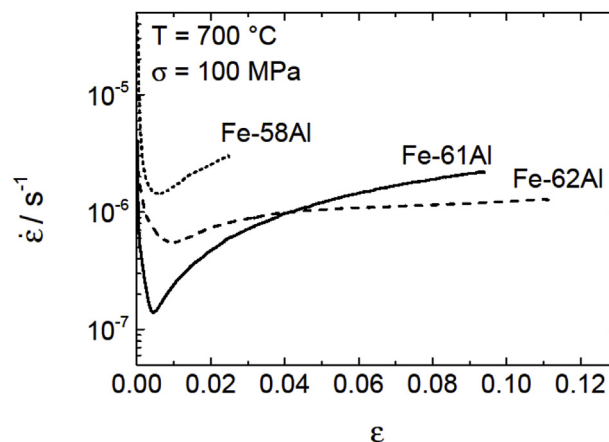


Fig. 14. Creep curves for off-eutectoid Fe-58Al and Fe-62Al as well as the fully lamellar, eutectoid Fe-61Al at 700 °C and an applied stress of 100 MPa [3].

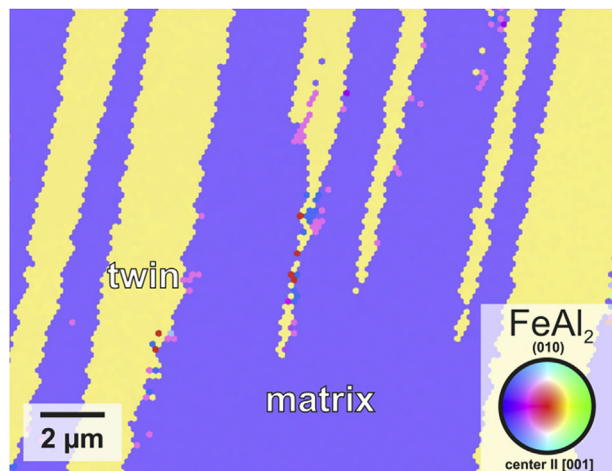


Fig. 13. Orientation imaging microscopy by EBSD on a cross section of crept, single-phase FeAl₂ alloy at 700 °C with an applied stress of 100 MPa showing the matrix grain in blue and yellow-colored deformation twins (color-coding according to the inverse pole figure of the compression direction in the inset). (For interpretation of the references to color in this figure legend, the reader is referred to the web version of this article.)

comprehensively characterize the deformed structure.

Within an individual colony, plastic deformation of FeAl dominates the early stages of creep prior to reaching a minimum creep rate while FeAl₂ exhibits elastic response. An increase in interfacial dislocation density accompanies this process. A minimum in creep rate signals the

commencement of the plastic deformation of FeAl₂, which deforms by slip and deformation twinning with (001) twin plane. This results in an increase in the creep rate. In the vicinity of the colony boundary, incompatibility resulting from lamellar misorientation between adjacent colonies results in localized plastic deformation that is manifested through dynamic recovery. This localization process eventually (with increasing global strain) leads to lamellae bending and fragmentation causing microstructural degradation and loss in creep resistance. It was possible to use these microstructural progressions to explain the experimentally observed creep response of off-eutectoid alloys as well.

Acknowledgement

The authors gratefully acknowledge funding by the Deutsche Forschungsgemeinschaft within the project “Fein-lamellare Fe-Al in-situ Kompositwerkstoffe” (HE 1872/26–2). MH and KSK acknowledge the Alexander von Humboldt Foundation for enabling this collaboration. This work was additionally supported by the Karlsruhe House of Young Scientists (KHYS, <http://www.khys.kit.edu/>). This work was carried out with the support of the Karlsruhe Nano Micro Facility (KNMF, www.knmf.kit.edu). Thanks are due to X. Li and F. Stein for providing the single-phase FeAl₂ alloy as well as K. Katela and D. Schliephake for assistance in TEM sample preparation and creep experiments, respectively.

Appendix A. Supplementary data

Supplementary data to this article can be found online at <https://doi.org/10.1016/j.intermet.2019.01.015>.

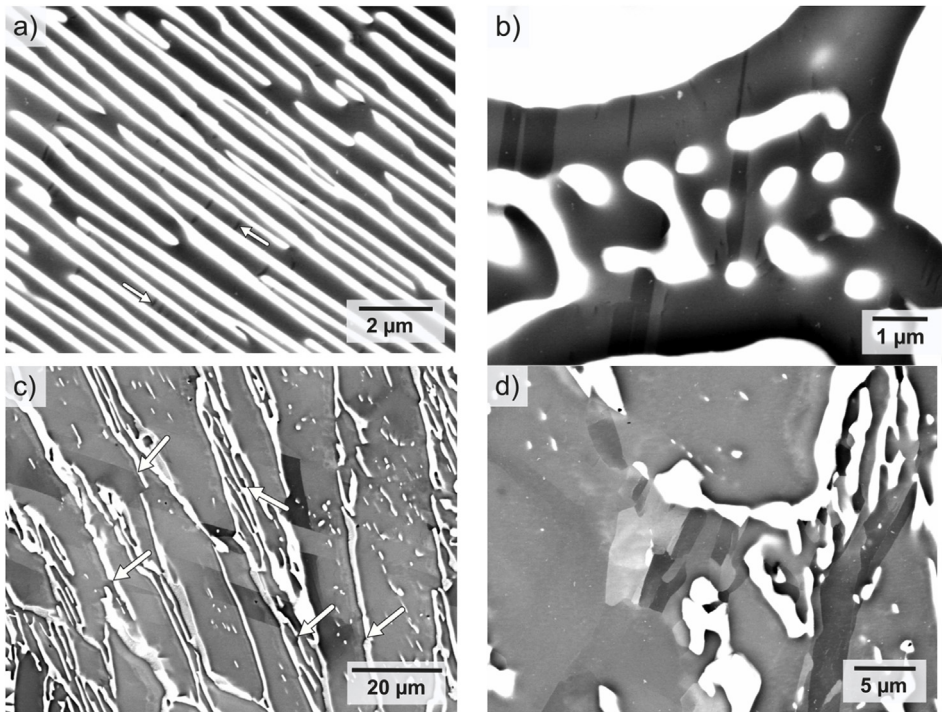


Fig. 15. Microstructure by SEM of the crept a,b) Fe-58Al and c,d) Fe-62Al at 700 °C and 100 MPa. The bright phase represents FeAl and the dark, FeAl₂. (a) and (b) show the presence of twins in FeAl₂ within the lamellar structure (highlighted by arrows in (a)) as well as in regions close to pro-eutectoid FeAl, respectively. Beside twins in FeAl₂ (see c), subgrains exist as well in as-crept Fe-62Al (d). Twins terminate at the FeAl/FeAl₂ interface and FeAl shows evidence for local deformation at these locations (highlighted by white arrows).

References

- [1] X. Li, A. Scherf, M. Heilmaier, F. Stein, The Al-rich part of the Fe-Al phase diagram, *J. Phase Equilibria Diffusion* 37 (2016) 162–173, <https://doi.org/10.1007/s11669-015-0446-7>.
- [2] M. Rank, P. Gotcu, P. Franke, H.J. Seifert, Thermodynamic investigations in the Al-Fe system: heat capacity measurements of three intermetallic phases, *Intermetallics* 94 (2018) 73–82, <https://doi.org/10.1016/j.intermet.2017.12.015>.
- [3] A. Schmitt, K.S. Kumar, A. Kauffmann, X. Li, F. Stein, M. Heilmaier, Creep of binary Fe-Al alloys with ultrafine lamellar microstructures, *Intermetallics* 90 (2017) 180–187, <https://doi.org/10.1016/j.intermet.2017.07.016>.
- [4] J. Albiez, I. Sprenger, C. Seemüller, D. Weygand, M. Heilmaier, T. Böhlke, Physically motivated model for creep of directionally solidified eutectics evaluated for the intermetallic NiAl-9Mo, *Acta Mater.* 110 (2016) 377–385, <https://doi.org/10.1016/j.actamat.2016.02.024>.
- [5] J.D. Whittenberger, R.D. Noebe, D.R. Johnson, B.F. Oliver, Compressive and tensile creep of a directionally solidified NiAl-14.5(at%)Ta alloy, *Intermetallics* 5 (1997) 173–183, [https://doi.org/10.1016/S0966-9795\(96\)00078-7](https://doi.org/10.1016/S0966-9795(96)00078-7).
- [6] D.R. Johnson, X.F. Chen, B.F. Oliver, R.D. Noebe, J.D. Whittenberger, Processing and mechanical properties of in-situ composites from the NiAlCr and the NiAl (Cr,Mo) eutectic systems, *Intermetallics* 3 (1995) 99–113, [https://doi.org/10.1016/0966-9795\(95\)92674-0](https://doi.org/10.1016/0966-9795(95)92674-0).
- [7] J.-M. Yang, The mechanical behavior of in-situ NiAl-refractory metal composites, *J. Min., Met. Mat. Soc.* 49 (1997) 40–43, <https://doi.org/10.1007/BF02914401>.
- [8] W.J. Zhang, S.C. Deevi, Analysis of the minimum creep rates of TiAl alloys, *Mater. Sci. Eng. A* 362 (2003) 280–291, [https://doi.org/10.1016/S0921-5093\(03\)00589-6](https://doi.org/10.1016/S0921-5093(03)00589-6).
- [9] M. Es-souni, A. Bartels, R. Wagner, Creep behaviour of a fully transformed near γ -TiAl alloy Ti-48Al-2Cr, *Acta Metall. Mater.* 43 (1995) 153–161, [https://doi.org/10.1016/0956-7151\(95\)90270-8](https://doi.org/10.1016/0956-7151(95)90270-8).
- [10] C.E. Wen, K. Yasue, J.G. Lin, Y.G. Zhang, C.Q. Chen, The effect of lamellar spacing on the creep behavior of a fully lamellar TiAl alloy, *Intermetallics* 8 (2000) 525–529, [https://doi.org/10.1016/S0966-9795\(99\)00131-4](https://doi.org/10.1016/S0966-9795(99)00131-4).
- [11] T.A. Parthasarathy, M.G. Mendiratta, D.M. Dimiduk, Flow behavior of PST and fully lamellar polycrystals of Ti-48Al in the microstrain regime, *Acta Mater.* 46 (1998) 4005–4016, [https://doi.org/10.1016/S1359-6454\(98\)00067-6](https://doi.org/10.1016/S1359-6454(98)00067-6).
- [12] L.M. Hsiung, T.G. Nieh, The evolution of deformation substructure in a creep deformed fully-lamellar TiAl alloy, *Mater. Sci. Eng. A* 239–240 (1997) 438–444, [https://doi.org/10.1016/S0921-5093\(97\)00614-X](https://doi.org/10.1016/S0921-5093(97)00614-X).
- [13] J. Meija, T.B. Coplen, M. Berglund, W.A. Brand, B.P. De, M. Gröning, N.E. Holden, J. Irrgeher, R.D. Loss, T. Walczyk, T. Prohaska, Atomic weights of the elements 2013 (IUPAC technical report), *Pure Appl. Chem.* 88 (2016) 265–291, <https://doi.org/10.1515/pac-2015-0305>.
- [14] A. Scherf, A. Kauffmann, S. Kauffmann-Weiss, T. Scherer, X. Li, F. Stein, M. Heilmaier, Orientation relationship of eutectoid FeAl and FeAl₂, *J. Appl. Crystallogr.* 49 (2016) 442–449.
- [15] A. Scherf, D. Janda, M.B. Yazdi, X. Li, F. Stein, M. Heilmaier, Oxidation behavior of binary aluminium-rich Fe-Al alloys with a fine-scaled, lamellar microstructure, *Oxid. Metals* 83 (2015) 559–574, <https://doi.org/10.1007/s11085-015-9535-6>.
- [16] F.D. Fischer, F. Appel, H. Clemens, A thermodynamical model for the nucleation of mechanical twins in TiAl, *Acta Mater.* 51 (2003) 1249–1260, [https://doi.org/10.1016/S1359-6454\(02\)00504-9](https://doi.org/10.1016/S1359-6454(02)00504-9).
- [17] Y. Umakoshi, M. Yamaguchi, Deformation of FeAl single crystals at high temperatures, *Philos. Mag. A* 41 (1980) 573–588, <https://doi.org/10.1080/01418618008239334>.
- [18] M.G. Mendiratta, H.-M. Kim, H.A. Lipsitt, Slip directions in B2 Fe-Al alloys, *Metall. Trans. A* 15 (1984) 395–399, <https://doi.org/10.1007/BF02645127>.
- [19] I. Baker, D.J. Gaydos, Flow and fracture of Fe-Al, *Mater. Sci. Eng.* 96 (1987) 147–158, [https://doi.org/10.1016/0025-5416\(87\)90549-0](https://doi.org/10.1016/0025-5416(87)90549-0).
- [20] Z.-J. Wang, Q.-J. Li, Y. Li, L.-C. Huang, L. Lu, M. Dao, J. Li, E. Ma, S. Suresh, Z.-W. Shan, Sliding of coherent twin boundaries, *Nat. Commun.* 8 (2017) 1108, <https://doi.org/10.1038/s41467-017-01234-8>.
- [21] J.A. Jimenez, G. Frommeyer, Creep behavior of intermetallic FeAl and FeAlCr alloys, *Mater. Sci. Eng. A* 220 (1996) 93–99, [https://doi.org/10.1016/S0921-5093\(96\)10480-9](https://doi.org/10.1016/S0921-5093(96)10480-9).